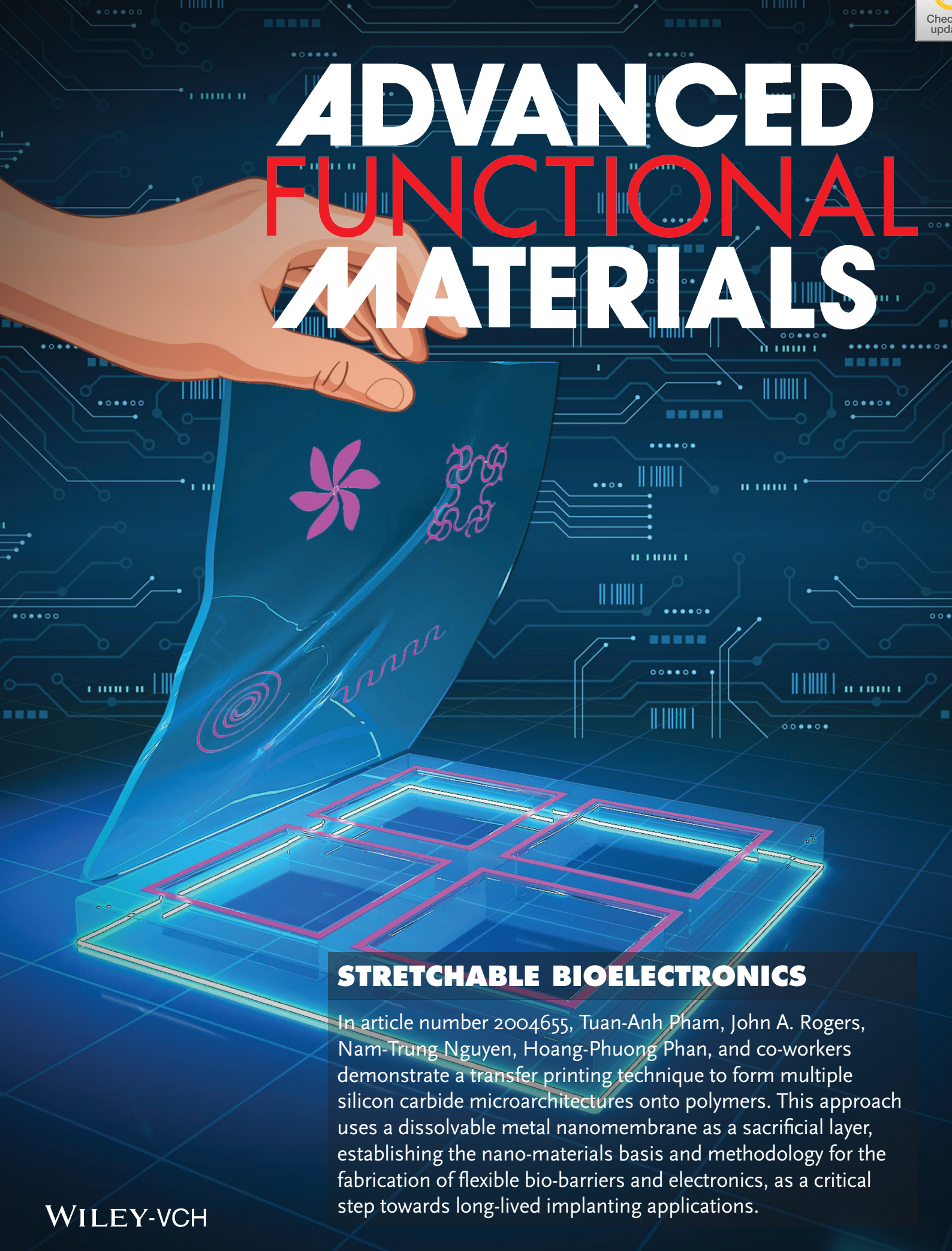


ADVANCED FUNCTIONAL MATERIALS

An illustration showing a hand holding a flexible, blue, patterned material. The material has several distinct patterns: a purple flower-like shape, a purple wavy pattern, and a purple spiral. Below the hand, a substrate with a grid of microstructures is shown. The microstructures are arranged in a 2x2 grid and are highlighted with a glowing blue and purple outline. The background is a dark blue grid with various circuit-like patterns and lines.

STRETCHABLE BIOELECTRONICS

In article number 2004655, Tuan-Anh Pham, John A. Rogers, Nam-Trung Nguyen, Hoang-Phuong Phan, and co-workers demonstrate a transfer printing technique to form multiple silicon carbide microarchitectures onto polymers. This approach uses a dissolvable metal nanomembrane as a sacrificial layer, establishing the nano-materials basis and methodology for the fabrication of flexible bio-barriers and electronics, as a critical step towards long-lived implanting applications.

A Versatile Sacrificial Layer for Transfer Printing of Wide Bandgap Materials for Implantable and Stretchable Bioelectronics

Tuan-Anh Pham,* Tuan-Khoa Nguyen, Raja Kumar Vadivelu, Toan Dinh, Afzaal Qamar, Sharda Yadav, Yusuke Yamauchi, John A. Rogers,* Nam-Trung Nguyen,* and Hoang-Phuong Phan*

Improving and optimizing the processes for transfer printing have the potential to further enhance capabilities in heterogeneous integration of various sensing materials on unconventional substrates for implantable and stretchable electronic devices in biosensing, diagnostics, and therapeutic applications. An advanced transfer printing method based on sacrificial layer engineering for silicon carbide materials in stretchable electronic devices is presented here. In contrast to the typical processes where defined anchor structures are required for the transfer step, the use of a sacrificial layer offers enhances versatility in releasing complex microstructures from rigid donor substrates to flexible receiver platforms. The sacrificial layer also minimizes twisting and wrinkling issues that may occur in free-standing microstructures, thereby facilitating printing onto flat polymer surfaces (e.g., polydimethylsiloxane). The experimental results demonstrate that transferred SiC microstructures exhibit good stretchability, stable electrical properties, excellent biocompatibility, as well as promising sensing-functions associated with a high level of structural perfection, without any cracks or tears. This transfer printing method can be applied to other classes of wide bandgap semiconductors, particularly group III-nitrides and diamond films epitaxially grown on Si substrates, thereby serving as the foundation for the development and possible commercialization of implantable and stretchable bioelectronic devices that exploit wide bandgap materials.

1. Introduction

Implantable and stretchable bioelectronics systems are of great interest for personal biomedical applications, owing to their lightweight, low stiffness, excellent adhesion to tissue surfaces, and high levels of mechanical flexibility.^[1–3] A key feature of these devices lies in their capability for continuous monitoring of cellular and tissue activities in real-time, thus providing valuable information and actionable feedback for diagnosis and treatment of neurological disorders or cardiac diseases.^[4–8] In this context, the integration of sensing materials with flexible polymeric substrates is of the topmost importance, as the basis for platforms that mechanically and geometrically match to soft, curved, and moving biological tissues.^[9] Unfortunately, inorganic semiconductors cannot be directly fabricated on flexible polymeric substrates via standard manufacturing processes as polymeric materials are usually destroyed or degraded under harsh processing conditions, such as ultraviolet

T.-A. Pham, Dr. T.-K. Nguyen, Dr. T. Dinh, Dr. S. Yadav,
Prof. N.-T. Nguyen, Dr. H.-P. Phan
Queensland Micro and Nanotechnology Centre
Griffith University
Nathan, QLD 4111, Australia
E-mail: tuananh.pham2@griffithuni.edu.au;
nam-trung.nguyen@griffith.edu.au; h.phan@griffith.edu.au

Dr. R. K. Vadivelu
Department of Chemical Systems Engineering
The University of Tokyo
Bunkyo-ku, Tokyo 113-0033, Japan

Dr. T. Dinh
Department of Mechanical Engineering
University of Southern Queensland
Springfield, QLD 4300, Australia

Dr. A. Qamar
Electrical Engineering Department
University of Michigan
Ann Arbor, MI 48109, USA

 The ORCID identification number(s) for the author(s) of this article can be found under <https://doi.org/10.1002/adfm.202004655>.

Prof. Y. Yamauchi
School of Chemical Engineering
Australian Institute for Bioengineering and Nanotechnology
The University of Queensland
St Lucia Brisbane, QLD 4072, Australia

Prof. Y. Yamauchi
Department of Plant & Environmental New Resources
Kyung Hee University
Gyeonggi-do, Yongin 17104, South Korea

Prof. J. A. Rogers
Department of Materials Science and Engineering
Department of Biomedical Engineering
Department of Neurological Surgery
Department of Chemistry
Department of Mechanical Engineering
Department of Electrical and Computer Science
Center for Bio-Integrated Electronics
Simpson Querrey Institute for Nano/biotechnology
Northwestern University
Evanston, IL 60208, USA
E-mail: jrogers@northwestern.edu

DOI: 10.1002/adfm.202004655

illumination, elevated temperatures, and chemical corrosion.^[10] Therefore, the development of a reliable fabrication process to integrate sensing materials onto flexible substrates is imperative. In this regard, the transfer printing technique represents a powerful approach to transfer microstructures of sensing materials from a donor substrate to a receiver template with excellent degrees of selectivity and uniformity.^[11–18] The choice of materials covered by this technique is not only limited to inorganic semiconductors, but also includes carbon-based materials (e.g., graphene) and organic semiconductors.^[19–23] The printing process functions efficiently if the released microstructures attach to the mother wafer in a flat, planar configuration (e.g., cantilevers, doubly clamped beams, or membranes) via defined anchors to maximize good conformal contact between the stamp and the microstructures. Nevertheless, this approach can be cumbersome for microstructures that involve complex geometric shapes and large degrees of residual stresses (e.g., epitaxial film being grown at high temperatures).^[24,25] This limitation represents a technical barrier in the design and construction of certain important classes of implantable and stretchable bioelectronic devices.

Among various wide bandgap semiconductor materials for implantable and stretchable bioelectronic devices, silicon carbide (SiC) is emerging as an attractive candidate due to its chemical inertness and its stable mechanical and electrical properties.^[26–32] Compared to monocrystalline Si, SiC exhibits excellent semiconducting functionality and long-lived stability under immersion in simulated biofluid environments without additional encapsulation layers.^[11] These features make SiC well suited for integration in low-cost, reliable implantable, and stretchable sensing devices designed for interfacing with the human body for diagnostic and therapeutic functions. Despite these advantages, relatively few studies have been focused on the integration of SiC with polymeric substrates for such bioelectronic devices.^[33–35] For instance, amorphous SiC was recently grown on polyimide substrates using low deposition temperatures to form protective layers for flexible neural electrodes.^[36,37] However, amorphous SiC usually possesses a high density of defects and pinholes associated with low electrical conduction, as a key shortcoming for high-performance bioelectronic devices. With this in mind, we previously developed a fabrication process using strain concentration designs to transfer print crystalline cubic SiC nanomembranes from an Si wafer to a polyimide substrate.^[11] Despite these interesting results, this method might not be suitable for complex SiC microstructures such as serpentine, spirals, and other elaborated configurations, due to the requirement for anchoring sections and flat surfaces for printing. This challenge could hinder the use of SiC and other wide band gap family materials in multi-functional, stretchable, soft architectures.

Herein, we introduce a versatile approach to transfer various SiC microstructures with diverse sizes and shapes onto stretchable substrates without the need for defined anchor structures. In particular, we use a thin layer of aluminum (Al) on the backsides of a free-standing SiC nanomembrane on Si wafer prior to an inductively coupled plasma etching process. The Al film serves as a supporting layer that prevents the formation of wrinkles or buckling in the SiC microstructures that can arise from gradients in residual stress. As a result, the flat SiC

microstructures can be easily integrated into stretchable substrates by a standard transfer printing process at a high level of structural perfection without cracks or tears. Our experimental results reveal that the as-fabricated SiC stretchable devices exhibit excellent mechanical, electrical properties as well as good cell level biocompatibility and highly temperature sensitivity. Notably, this method can be applied to numerous inorganic semiconducting materials epitaxially grown on standard Si substrates. The outcome of this study has the potential to create important opportunities in the development of unusual implantable and stretchable bioelectronic devices for physiological signals sensing and treatment.

2. Results and Discussion

Figure 1 illustrates the concept of the transfer printing method to form multiple structures of stretchable and flexible electronic devices based on crystalline SiC. Prior to this fabrication flow, nanoscale films of SiC were grown on a silicon wafer using low pressure chemical vapor deposition. We deposited SiC films on both sides of the silicon wafer to balance the residual stress in the SiC films induced by the high-temperature CVD process, thereby preventing large-scale wafer bowing or cracking. Among various SiC polytypes, such as hexagonal (4H-SiC and 6H-SiC) and cubic (3C-SiC) crystals, we chose 3C-SiC because this crystal can be grown on an Si substrate, enabling its compatibility with conventional micro/nano-fabrication techniques as well as reducing material cost. The fabrication process starts with the formation of free-standing SiC nanomembranes by removing the back-side silicon carbide and silicon substrate using inductively coupled plasma (ICP) combined with KOH etching. Next, photolithography and top surface hard masks were patterned on the SiC nanomembranes to obtain different structures. Subsequently, another layer of aluminum was deposited onto the backside of the free-standing nanomembranes to create a sacrificial layer, helping to avoid the formation of wrinkles and twists in the structures. Undesirable parts of the SiC nanomembranes were then removed using the ICP etching. Subsequently, the patterned SiC structures along with the Al supporting film were printed onto a polydimethylsiloxane (PDMS) slab in a process that involved good conformal contact. Finally, the crystalline SiC microstructures on PDMS were detached from the Si substrate through Al etching and mechanical removal. This SiC microstructure printed on PDMS can be further transferred onto other flexible substrates (e.g., polyimide, SU8) for the construction of various implantable bioelectronic devices (step viii).

Figure 2 presents a visual comparison between SiC microstructures formed with and without the sacrificial Al layer. Without the supporting layer, free standing SiC microstructures (i.e., the spring shape) exhibit significant bending and twisting. This behavior is reasonable as the SiC film was epitaxially grown at high temperatures above 1000 °C, resulting in a large thermal stress upon cooling to room temperature.^[38–40] The difference between the lattice constants of SiC and Si (approximately 20%) also plays an important role in the formation of residual gradients of up to several hundred MPa in the SiC films, as reported previously in our studies.^[41,42]

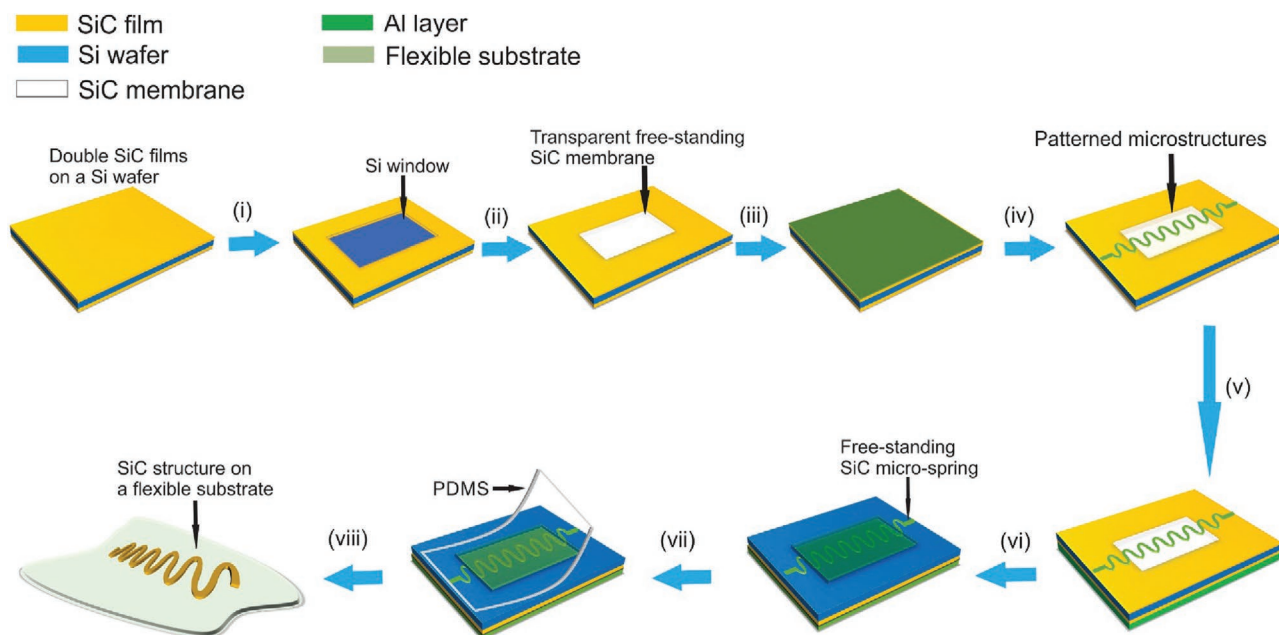


Figure 1. Steps for the transfer of diverse SiC microstructures from an Si wafer to a flexible substrate for stretchable bioelectronics using the transfer printing method employed with a sacrificial layer technique.

These twisting and bending phenomena are not desirable for the transfer printing process, because a flat configuration is essential for a good contact between the free-standing microstructures and surface of the PDMS slab. Indeed, the SiC micro-spring structure was cracked after transferring onto PDMS, as confirmed by optical microscopy (data not shown). Moreover, the close-up SEM image in Figure 2c reveals the co-existence of several sheet-like films located at the edges of the SiC micro-spring structure. These films could be related to residual SiC material after ICP etching of the SiC nanomembranes, confirming the inefficiency of the dry etching process in this case (see Figure S2, Supporting Information, for more information). This observation could be due to the twisted configuration of the SiC microstructures that hinders a maximum exposure of the structures to the incident beams bombarding the target surface in a normal direction. In contrast, the spring-shape structure displays a flat configuration as a result of the mechanical support from the Al sacrificial layer underneath as shown in Figure 2d,e, enabling the subsequent transfer printing process. Moreover, no residual SiC films were observed at the edges of the SiC micro-spring structure, as confirmed by a close-up SEM image shown in Figure 2f. This result suggests that the SiC nanomembranes were completely removed after the ICP etching process. Furthermore, to prove the versatility of this transfer method, we demonstrated a series of microstructures with different sizes and shapes, including gear, flower, and U-shaped microstructures. As expected, these microstructures are flat on the sacrificial layer, Figure 2g–l. These new class of defect-free SiC microstructure arrays transferred onto soft substrates may provide additional degrees of freedom in designing flexible applications (e.g., photonic crystals, metamaterials) using wide band gap materials.^[43–45] Particularly, our transfer method can be applied to other wide band gap materials, such as group III-nitrides or diamond films epitaxially grown on Si

substrates because the chemical inertness of these epitaxial films offer great compatibility with standard transfer printing methods to form desired complex microstructures, similar to our demonstration for the cubic SiC in this study.^[44,46]

We applied the transfer printing process to several complex geometric microstructures having the minimum line width of 10 μm , including spiral, serpentine, and propeller microstructures, and detached them from the host wafer by etching the sacrificial layer. Transferring these microstructures onto a soft substrate was not possible with the standard printing process since similar twisting phenomena as observed in the spring-shape are likely to occur. The compatibility with standard wafer-level microfabrication technologies enables large-scale, mass production of multiple flexible SiC structures in a single process, **Figure 3a–d**).

Figure 3f–h shows optical microscopy images of the spiral, serpentine, and propeller microstructures on SiC nanomembranes after lithography process. After removing SiC nanomembranes by ICP etching, these microstructures remain flat with the mechanical support from the Al sacrificial layer underneath, as confirmed by SEM images, Figure 3i–k. Another significant benefit of the Al layer is that it can be quickly dissolved in a wet etchant ($\text{H}_3\text{PO}_4\text{:HNO}_3\text{:CH}_3\text{COOH}$), leaving the chemically inert SiC microstructures on PDMS. A digital photograph shown in Figure 3d illustrates the printing step in which the PDMS slab was gently peeled off from the donor substrate. Figure 3l–n shows SEM images of the SiC spiral, serpentine, and propeller microstructures on a PDMS slab (coated by a thin metallic layer for SEM), confirming no signs of cracks or tears in these SiC microstructures. The wrinkled background that appears around and underneath these SiC microstructures originates from the metallic layer required to avoid charging effects in the SEM images. Figure 3e shows Raman spectra of the SiC microstructures before and after transferring onto the PDMS

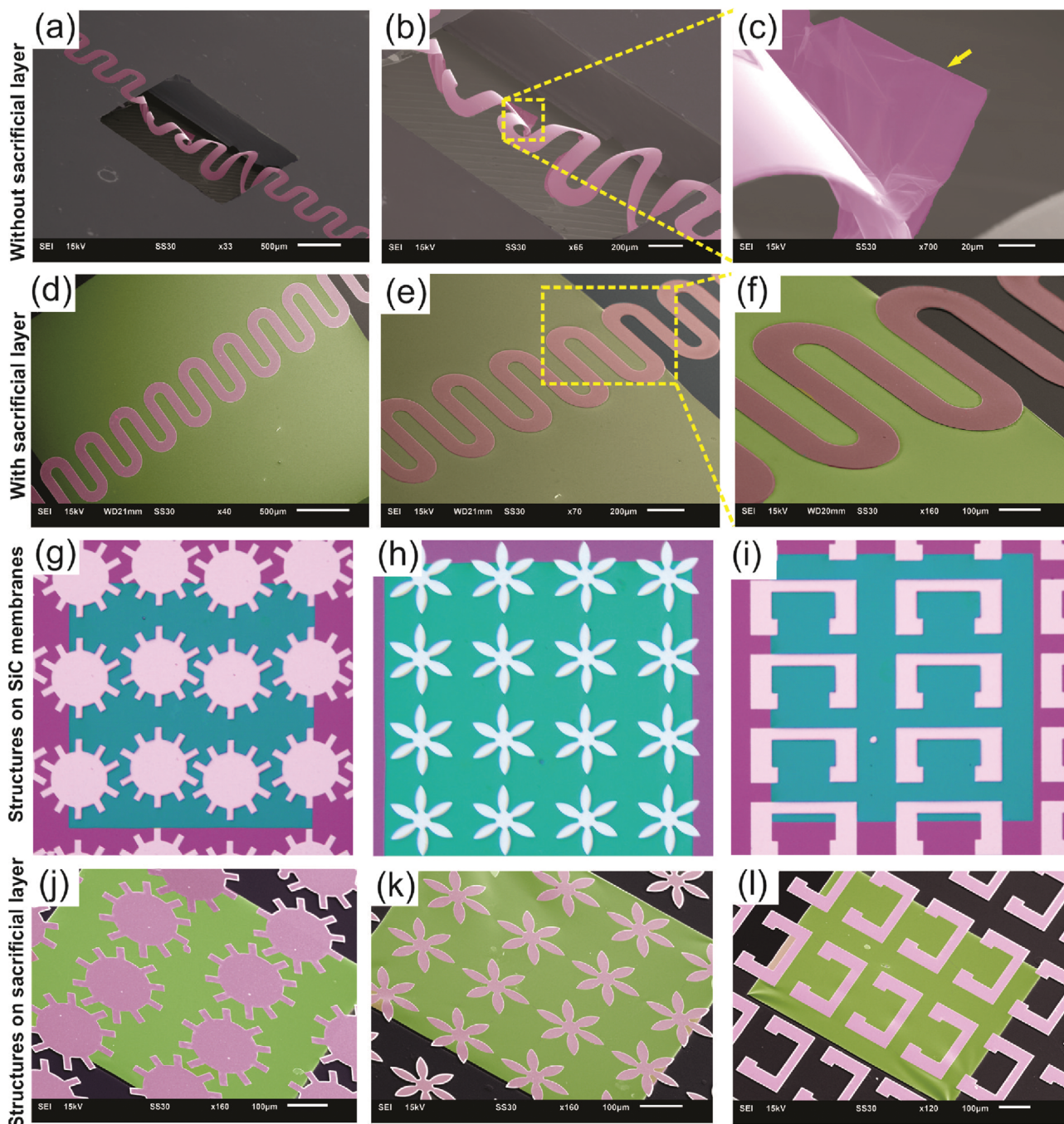


Figure 2. Thin SiC structures. SEM images of the SiC micro-spring structures obtained a–c) without and d–f) with the sacrificial layer. g–l) Optical microscopy images and SEM images of various microstructures laying on the aluminum sacrificial layer, respectively: gear (left), flower (middle), and U (right)-shaped structures. The yellow arrow in (c) marks the presence of residual SiC after the ICP etching.

substrate. The data indicate no significant shifts between the two spectra, with a similar transverse optical vibration wavelength of 796 cm^{-1} . This result further confirms the excellent degree of structural perfection of the SiC microstructures after transferring onto the PDMS substrate. The intriguing results above unambiguously demonstrate the success of our approach, as an important progress in the transfer of diverse microstructures from rigid substrates onto flexible polymeric substrates

for the development of the next generation of reliable bioelectronic devices. Among these applications, integration of electronics into Organ-on-Chip (OOC) platforms is of increasing interest as a powerful approach to culturing cells to mimic and emulate functional units of human organs.^[47,48] SiC-stretchable electronics can be considered as an ideal platform for OOC due to its optical transparency for fluorescent observation, along with multiple functionalities that enable probing cell behaviors.

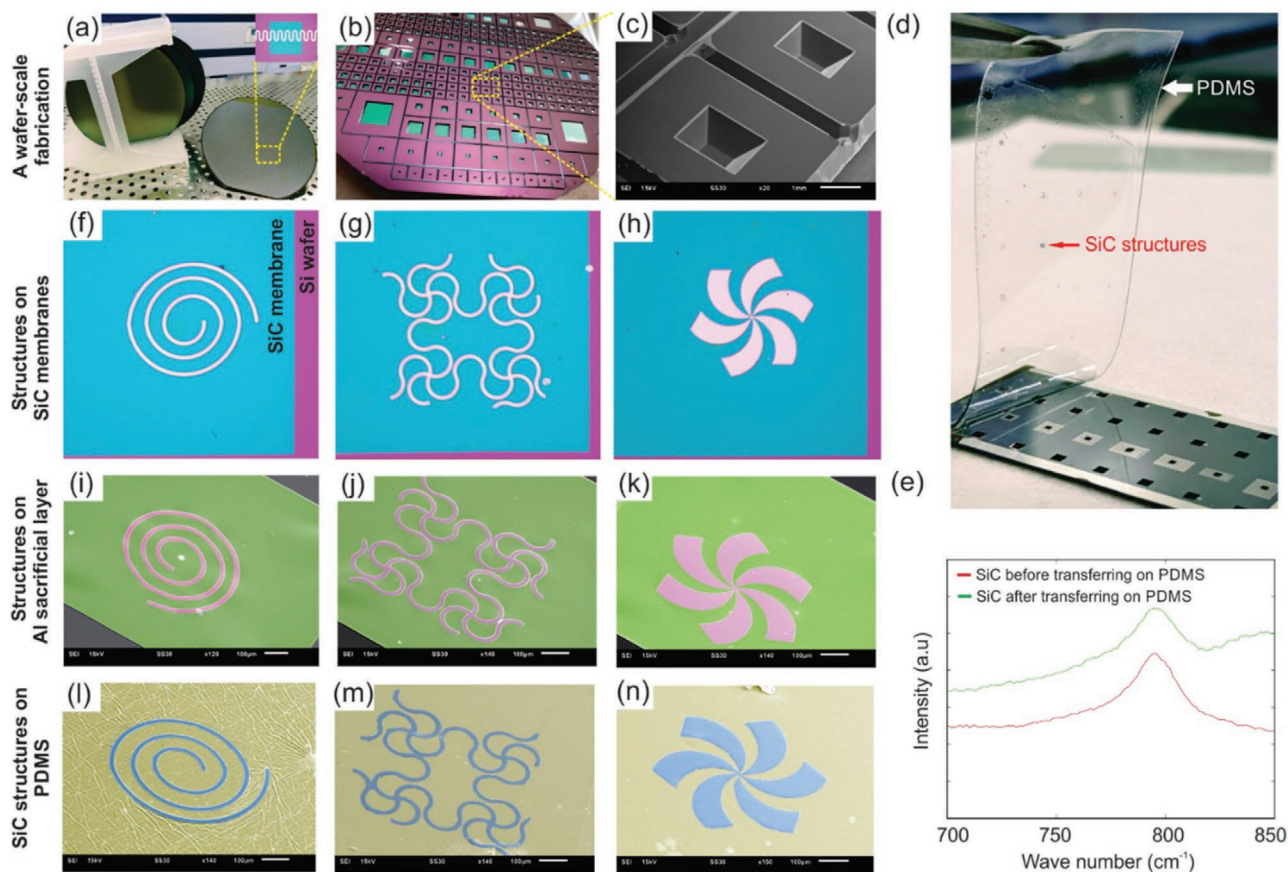


Figure 3. a) Images of SiC films grown on a 6 in. Si substrate. Inset in (a) shows the SiC micro-spring structures formed on the SiC membrane after the fabrication. b,c) Wafer level fabrication of free-standing SiC nanomembranes where an SiC layer grown on the back side of Si was utilized as the hard mask for Si wet-etching and the corresponding SEM image of an SiC nanomembrane, respectively. d) Digital photograph represents the peeling-off of the PDMS slab containing SiC microstructures from the donor substrate. SiC microstructure can be seen by naked eye as indicated by the red arrow. f–h) Optical microscopy images of spiral, serpentine, and propeller microstructures laying on SiC nanomembranes, respectively. SEM images of these microstructures laying on i–k) the Al sacrificial layer and l–n) PDMS substrate, respectively. e) Raman spectra of the SiC microstructure before and after transferring from the rigid Si substrate to the PDMS substrate.

We performed experiments to examine the stretchability and deformability of SiC-on-PDMS as a proof of concept for OOC applications. Finite element analysis (FEA) method shows that using a spring-shape structure can reduce the effective strain induced into SiC. As such, under an applied strain of approximately 4000 ppm, the maximum strain occurs at the curved regions of the spring, and is diminished down to 1000 ppm, **Figure 4a**. Based on this design, we fabricated an SiC spring with dimension of 5 mm in length and 100 μm in width, printed onto a PDMS membrane with a thickness of 125 μm . Notably, no cracks were observed when the SiC-on-PDMS membrane was wrapped around a cylinder tube with diameter of 8 mm, indicating good flexibility, **Figure 4b** (see **Figure S3**, Supporting Information, for more information). The SiC spring on PDMS was then mounted onto an enclosed chamber, where air pressure was applied to deform the membrane into a dome shape. The pressure needed to generate desired strain into the SiC micro-spring was explored using a simulation model for the deformation of the PDMS membrane (see **Figure S1**, Supporting Information, for more information). The deflection h of the membrane was given by $\Delta l/l_0 = 2.15 \times (h/l_0)^2$ where l_0 is

the initial length of the SiC micro-spring structure before deformation,^[49] as shown in **Figure 4c**. The experimental setup to examine the stretchability of the SiC micro-spring structure is shown in **Figure 4d,e** (refer to the stretchable test in the Experimental Section for detailed information). Under an applied pressure of 6 mbar, the OOC membrane experiences a large out-of-plane deflection of 240 μm , suitable for applications such as cell stretching and mechano-transducing. **Figure 4f,g** shows the current–voltage (I – V) characteristic curves and the resistance modulation of the SiC micro-spring structure as a function of a number of test cycles under a differential pressure of 6 mbar. The results show that there is no significant change in the resistance of the SiC micro-spring structure when deformed to a deflection of $\approx 240 \mu\text{m}$ up to 1000 test cycles. Increasing the differential pressure to 18 mbar results in a larger deflection as clearly observed by naked eye (refer to the video in the Supporting Information) but does not lead to any significant changes in the resistance of the SiC spring microstructure as shown in **Figure 4h,i**. These electrical measurements confirm an excellent level of stretchability and deformability of the SiC micro-spring structures after transferring onto PDMS.

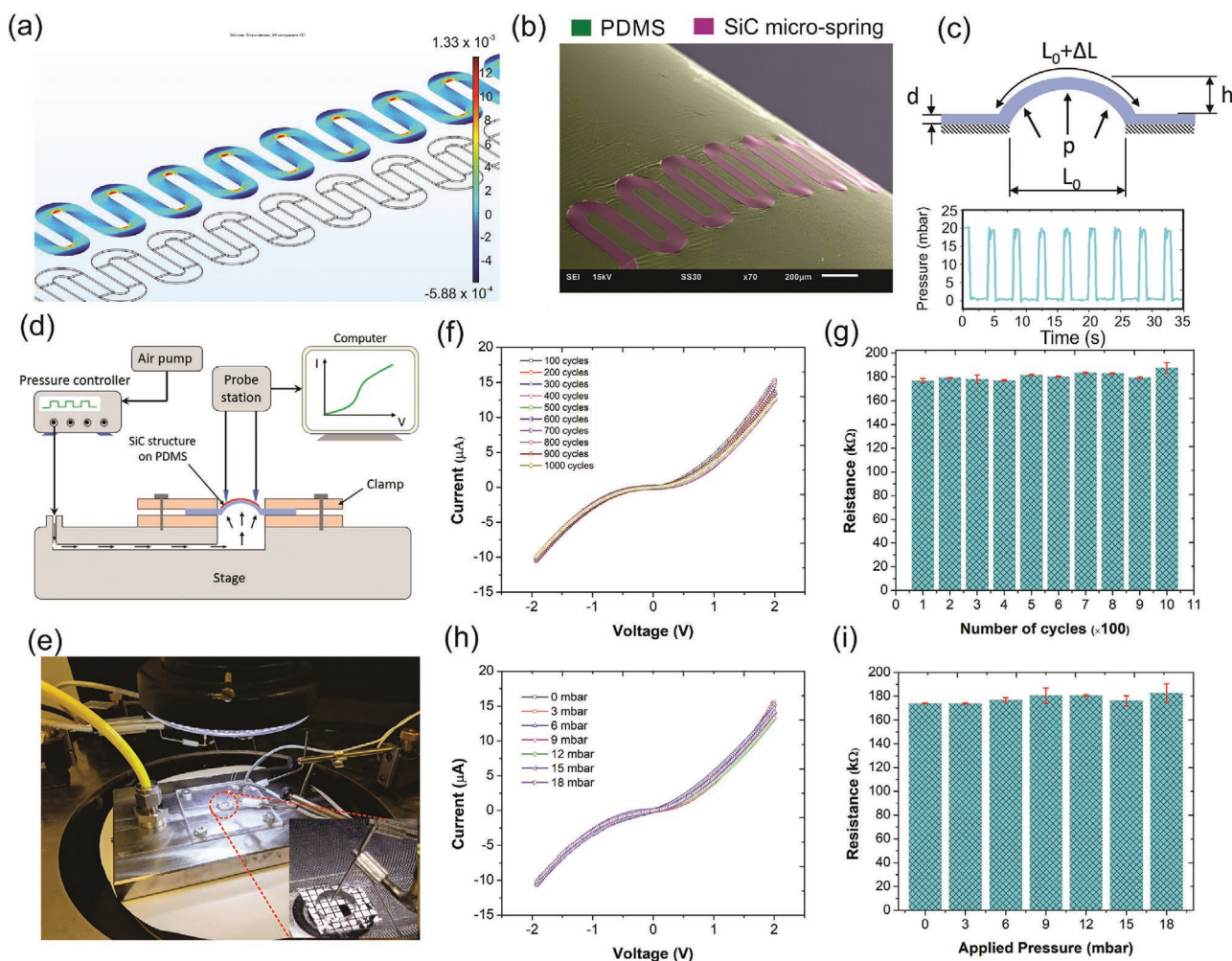


Figure 4. a) Finite element analysis simulation shows that using a spring-shape structure can reduce the effective strain induced into SiC. b) SEM images of the SiC spring/PDMS membrane under mechanical deformation. c) Cross section of an SiC spring/PDMS membrane for calculating the deflection h induced by the differential pressure (top) and the pressure pulse applied to the membrane (bottom). d,e) A cartoon illustration and digital photograph show the experimental setup to investigate the stretchability of the SiC spring microstructure after transferring onto the PDMS membrane, respectively. f–i) Current–voltage characteristic curves and the corresponding resistance modulations of the SiC spring microstructures recorded at different number of test cycles and differential pressure levels.

To examine the possibility to construct multifunctional SiC flexible electronic devices for their use in biomedical applications, such as temperature monitoring, we fabricated a flexible temperature sensor via the fabrication process described above. For this, low-doped SiC is most useful because it offers improved temperature sensitivity compared to that of highly doped samples. **Figure 5a** shows the I – V characteristic curves of the as-fabricated sensing device recorded at different temperatures. These I – V curves indicate that the current increases with temperature, consistent with a negative temperature coefficient. Notably, the temperature sensing mechanism of the device relies on the thermoresistive effect in SiC, which is associated with a thermally activated mobility of charge carriers (μ), described by an Arrhenius-type equation, $\mu \propto \exp[-E_A/k_B T]$, where E_A stands for the activation energy and k_B is the Boltzmann constant.^[50] The temperature coefficient of resistance (TCR) is calculated as $TCR = \Delta R/R_0 \times 1/\Delta T$. **Figure 5b** plots the

$\Delta R/R$ and TCR as a function of temperature from 25 to 55 °C. The result shows a high TCR at approximately $-24\,000\text{ ppm K}^{-1}$ at 35 °C, which is much higher than that of several materials used for the fabrication of sensing devices, such as gold (3400 ppm K^{-1}) or platinum (3920 ppm K^{-1}).

For implantable electronics and OOC applications, the sensing materials must be biocompatible.^[51] The SiC surface is an inert, non-toxic contact site that allows cells to firmly attach, proliferate, and then eventually spread to establish cell–cell contact. SiC-on-PDMS exhibits an excellent level of optical transparency, to facilitate optical imaging (**Figure 6a,b**). The average optical transmittance of 230 nm-thick SiC on 125 μm -thick PDMS is higher than 60%, at least three times larger than that of ultra-thin amorphous Si films (20 nm-thick). Using these SiC-based OOC devices, we investigated the physiological and morphological features of HDF on the SiC surface. The growth of HDF indicated viability similar to that of standard

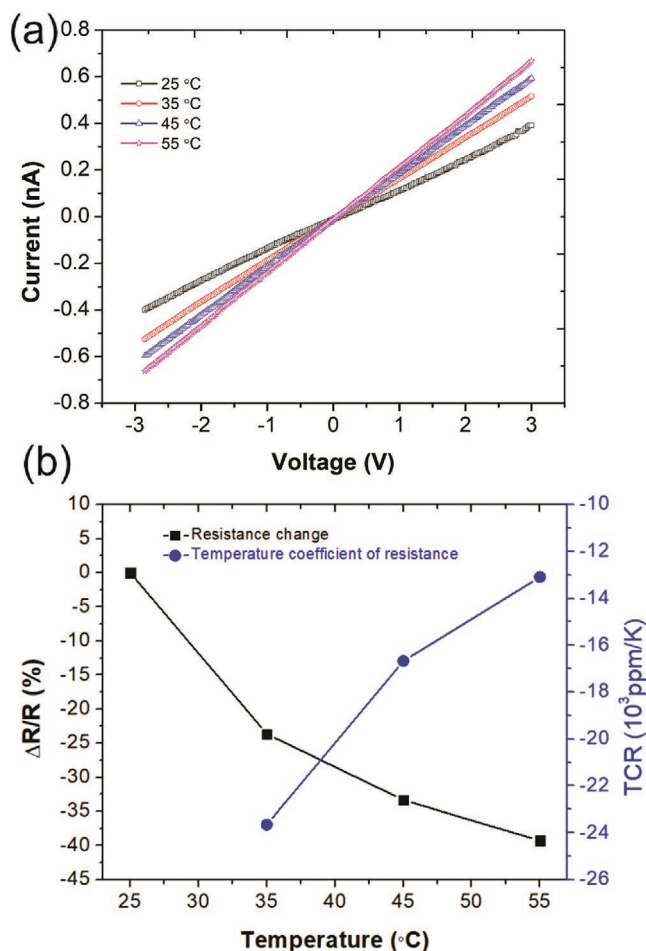


Figure 5. a,b) I - V characteristic curves and the corresponding TCR of the SiC/PDMS temperature sensing device obtained via the fabrication process that exploits sacrificial layer engineering.

dishes during prolonged cultures up to 72 h (Figure 6c,d). In addition, Live/Dead staining showed no cytotoxic effects such as significant apoptotic or necrotic features (Figure 6e). The SiC also demonstrates a protective effect on mitochondria. The cells display good distribution of mitochondria, consistent with the existence of healthy function without signs of mitotoxicity (Figure 6f).

Next, we investigated the regulation of actin dynamics in cells that adhere on SiC surface. The attached cells exhibited flattened morphology and persisted to spread, as supported by actin polymerization. As shown in Figure 6g, at 24 h after seeding, an enhanced formation of actin stress fibers occurred, which displays formation of protrusive lamella at the cell leading edge. Over the course of the next 24 h, cells widely spread with actin assembling into straight, long bundles. Intriguingly, the actin filaments organize into branched arrays at 72 h. More importantly, such evidence of actin organization provides a means to effectively support cell-cell contact. Overall, this investigation indicates cytological compatibility of SiC and appropriateness for the use of culturing cells for extended duration, demonstrating the potential of flexible SiC electronics for OOC and implantable applications.

3. Conclusion

This study introduces a versatile transfer printing process that employs a thin aluminum film as a sacrificial layer to facilitate release and transfer diverse SiC microstructures from rigid Si wafers onto flexible PDMS substrates. The transferred SiC microstructures exhibit a high degree of structural perfection without cracks or tears while maintaining good semi-conducting functionality, biocompatibility, stretchability, and deformability as unambiguously demonstrated by a comprehensive set of measurements. The key merits of the present work are the elimination of defined anchors and the minimization of twisting and bending in released microstructures. These features enabled the integration of a variety of microstructures onto flexible substrates at the wafer-scale level, regardless of the sizes and shapes and perhaps with applicability to other classes of materials (e.g., GaN and diamond-like carbon which are epitaxially deposited on Si wafers). Our findings, therefore, can be viewed as an important step in the mass production of diverse implantable and stretchable bioelectronic devices using the transfer printing fabrication process, with potential applications in physiological signal sensing and disease treatment.

4. Experimental Section

Deposition of SiC Films on Si Wafers: SiC films were deposited onto Si substrates using a hot wall chamber (Epiflex) at a temperature of 1250 °C. Prior to thin film deposition, the Si substrate was cleaned using the standard process RCA (Radio Corporation of America). The growth process started with carbonization of the Si surface followed by an alternating supply of epitaxy cycles where SiH_4 and C_2H_6 were utilized as Si and C precursors. To form n-type and p-type SiC, an in situ doping method was employed in which NH_3 and TMAI were the dopants for n-type and p-type, respectively.

Fabrication of Free-Standing SiC Nanomembranes: The backside SiC layer was used as a hard mask to form free-standing nanomembranes on the top surface. The AZ5214 photoresist was spin-coated and then patterned to form microscale window structures on the SiC bottom layer. This SiC bottom layer was then dry-etched using inductively coupled plasma etching ($\text{SF}_6 + \text{O}_2$) for about 2 min to expose the silicon layer. The exposed area of this silicon layer was then wet-etched using KOH (30%) at 80 °C for 10 h, leaving square-shaped free-standing SiC nanomembranes.

Device Fabrication Process: The wafer supporting free-standing SiC nanomembranes was cleaned using RCA to remove Si contamination. Next, 200 nm aluminum was deposited on the free-standing SiC films to form a hard mask for subsequent SiC plasma etching. The AZ5214 photoresist was spin-coated on Al/Si and patterned on free-standing membranes to form various microstructures, including spring, gear, flower, serpentine, spiral, and propeller-shaped structures. Then, another aluminum film was deposited at the bottom side of the patterned wafer to form a sacrificial layer. The exposed SiC areas were then plasma-etched, leaving free-standing Al/SiC microstructures laying on the aluminum sacrificial layer. The Al/SiC microstructures were then transferred onto PDMS slabs via a printing step. The aluminum layers from the mask and sacrificial layer were then removed using wet-etching to obtain SiC spring microstructures on PDMS slab. Detailed information of the fabrication process can be found in the Supporting Information.

SEM Measurements: SEM images were recorded using a JEOL JSM 6510 instrument (Japan) with an accelerating voltage of 15 kV. The samples were placed on a sample holder before inserting into the instrument. Before SEM measurements, a thin film of aluminum was

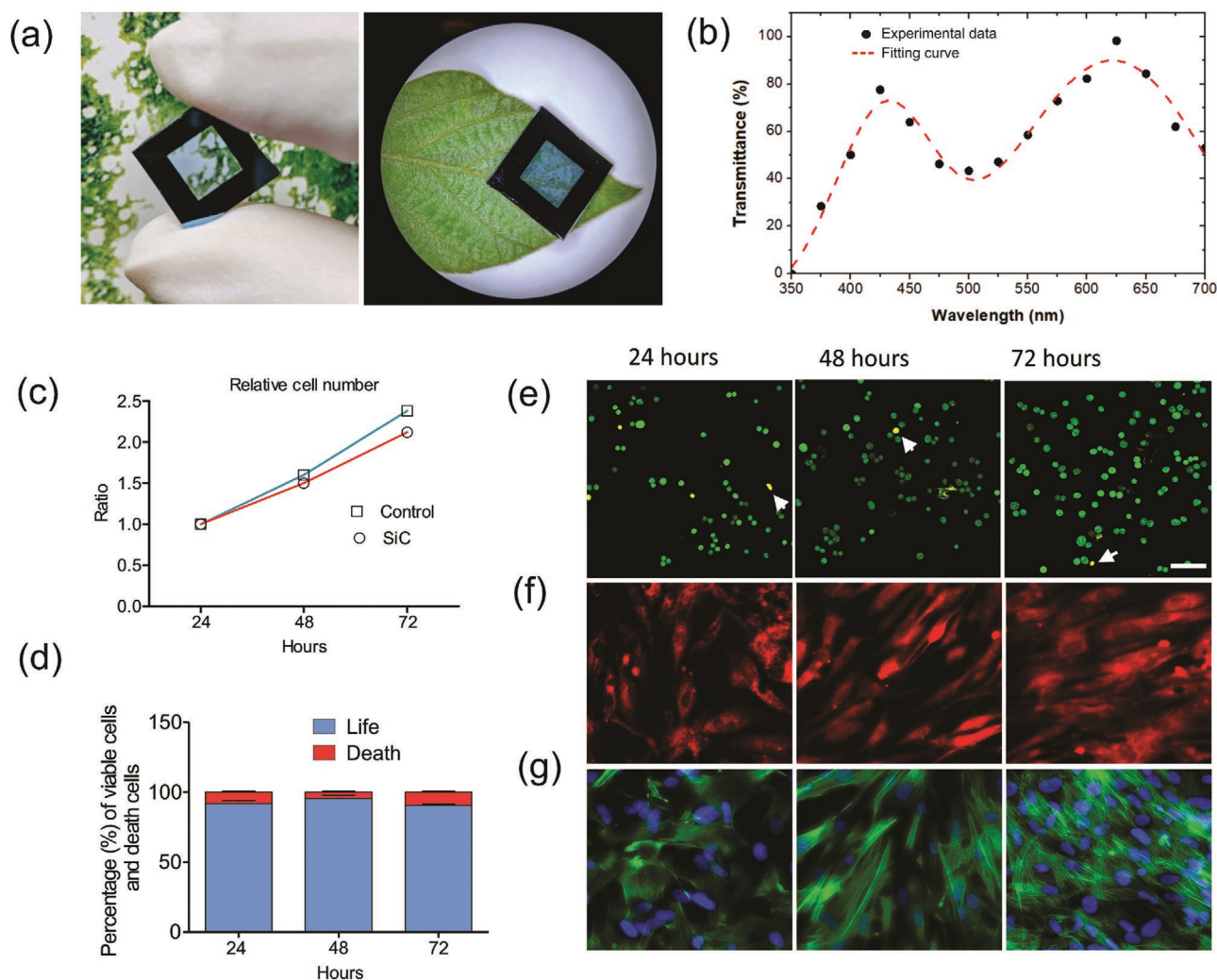


Figure 6. a,b) A digital photograph and optical transmittance curve, showing an excellent transparency of the 200 nm SiC membranes. c,d) Cytocompatibility and growth HDF on SiC. The cell showed no significant differences in viability at 24, 48, and 72 h (c). e) Fluorescence micrograph of AO/PI double-stained; green indicates live cells and yellow indicates death cells as marked by white arrow heads. f) Staining MitoTracker Red CMXRos, suggesting that biogenesis of mitochondria is prominent with the cell growth; leading to a maintenance of cellular viability. g) Representative images of HDF co-localization with actin (green) and nucleus (blue) showing actin cytoskeleton arrangement is associated with cell attachment and spreading at 24 h; formation of straight long actin bundle at 48 h and branching actin network formed at 72 h. Scale bars: 50 μm .

deposited onto the sample surface by sputter deposition to prevent the accumulation of electrostatic charge at the sample surface during the measurements.

Stretchable Test: The SiC-spring/PDMS membrane was sandwiched between the two thin hole-plates of acrylic. This sandwiched structure was then placed and secured on a vacuum chamber bearing a similar hole with the acrylic plates using screwed nuts. The pump and pressure controller were used (Eveflow OB1 MK3+) to generate a differential pressure to the SiC-spring/PDMS membrane in a controllable manner. The cycling test was performed using a square-shape pressure function, with an interval of 3 s for each cycle.

Electrical Measurements: The current–voltage (I – V) characteristics of all samples were measured using a semiconductor device parameter analyzer (Agilent B1500). The temperature sensors were examined using a thermal chuck where electrical contact was formed using a probe station. The temperature of the SiC/PDMS samples was calibrated with respect to a PDMS reference sample having the same thickness.

Cell Culture, Live/Dead Tests, and Morphology: The human dermal fibroblast (HDF) cells were cultured using T25 flasks at 37 $^{\circ}\text{C}$ in a

humidified incubator inclusive of 5% carbon dioxide in DMEM/F12 with phenol red indicator supplemented with 10% FBS and 1% penicillin/streptomycin. For the biocompatibility tests, 2×10^4 cells were seeded on an SiC membrane which was placed inside each well of 24-well plate. Following incubation, culture supernatant containing detached cells and adherent cells were subjected to the viability test. Aliquots of 20 μL of cells to 20 μL of 0.4% trypan blue were suspended and the mixture was incubated at room temperature for 2 min. The TB exclusion test was then performed by counting live (un-stained) and dead (stained) cells in a Neubauer chamber. The live/dead profiles at each culture time point were detected by staining small aliquot of cells with fluorescent dyes; 5 μL of acridine orange ($10 \mu\text{g mL}^{-1}$) + 5 μL propidium iodide ($10 \mu\text{g mL}^{-1}$). Representative fluorescent images indicated AO-stained (green) live cells and PI-stained (red/orange) dead cells. For morphological investigations, the SiC membrane was stained with fluorescent dyes: 1) MitoTracker CMXRos (Invitrogen) to detect mitochondrial distribution; 2) The cytoskeleton reorganization and the nuclei profile were examined by staining with ActinGreen 488 and NucBlue ReadyProbes reagents (ThermoFisher Scientific, Inc., Australia). The fluorescent imaging was

carried using an inverted fluorescent microscope (Nikon eclipse Ti2, Nikon Corporation, Tokyo, Japan).

Supporting Information

Supporting Information is available from the Wiley Online Library or from the author.

Acknowledgements

This work was partially funded by the discovery grant DE200100238 from the Australian Research Council (ARC). The 3C-SiC material was developed and supplied by Leonie Hold and Alan Iacopi of the Queensland Microtechnology Facility, part of the Queensland node, Griffith of the Australian National Fabrication Facility, a company established under the National Collaborative Research Infrastructure Strategy to provide nano- and microfabrication facilities for Australia's researchers.

Conflict of Interest

The authors declare no conflict of interest.

Keywords

bio-integrated electronics, Nano Electro Mechanical Systems (NEMS), sacrificial layers, sensing devices, stretchable substrates, transfer printing

Received: May 31, 2020

Revised: June 22, 2020

Published online: September 4, 2020

- [1] T. Dinh, T. Nguyen, H.-P. Phan, T.-K. Nguyen, V. T. Dau, N.-T. Nguyen, D. V. Dao, *Small* **2020**, *16*, 1905707.
- [2] D. Kuzum, H. Takano, E. Shim, J. C. Reed, H. Juul, A. G. Richardson, J. D. Vries, H. Bink, M. A. Dichter, T. H. Lucas, D. A. Coulter, E. Cubukcu, B. Litt, *Nat. Commun.* **2014**, *5*, 5259.
- [3] T.-M. Fu, G. Hong, R. D. Viveros, T. Zhou, C. M. Lieber, *Proc. Natl. Acad. Sci. USA* **2017**, *21*, 114.
- [4] J. W. Jeong, J. G. MacCall, G. Shin, Y. Zhang, R. Al-Hasani, M. Kim, S. Li, J. Y. Sim, K. I. Jang, Y. Shi, D. Y. Hong, Y. Liu, G. P. Schimitz, L. Xia, Z. He, P. Gamble, W. Z. Ray, Y. Huang, M. R. Bruchas, J. A. Rogers, *Cell* **2015**, *162*, 662.
- [5] X. Dai, W. Zhou, T. Gao, J. Liu, C. M. Lieber, *Nat. Nanotechnol.* **2016**, *11*, 776.
- [6] J. J. Jun, N. A. Steinmetz, J. H. Siegle, D. J. Denman, M. Bauza, B. Barbarits, A. K. Lee, C. A. Anastassiou, A. Andrei, C. Aydin, M. Barbic, T. J. Blanche, V. Bonin, J. Couto, B. Dutta, S. L. Gratiy, D. A. Gutnisky, M. Hausser, B. Karsh, P. Ledochowitsch, C. M. Lopez, C. Mitelut, S. Musa, M. Okun, M. Pachitariu, J. Putzeys, P. D. Rich, C. Rossant, W. L. Sun, K. Svoboda, et al., *Nature* **2017**, *551*, 232.
- [7] E. Formento, K. Minassian, F. Wagner, J. B. Mignardot, C. G. Le Goff-Mignardot, A. Rowald, J. Bloch, S. Micera, M. Capogrosso, G. Courtine, *Nat. Neurosci.* **2018**, *21*, 1728.
- [8] T. Someya, Z. Bao, G. G. Malliaras, *Nature* **2016**, *540*, 379.
- [9] J. Viventi, D. H. Kim, J. D. Moss, Y.-S. Kim, J. A. Blanco, N. Annetta, A. Hicks, J. L. Xiao, Y. Huang, D. J. Callans, J. A. Rogers, B. A. Litt, *Sci. Transl. Med.* **2010**, *2*, 2422.
- [10] V. M. Pathak, Navneet, *Bioresour. Bioprocess.* **2017**, *4*, 15.
- [11] H.-P. Phan, Y. Zhong, T.-K. Nguyen, Y. Park, T. Dinh, E. Song, R. K. Vadivelu, M. K. Masud, J. Li, M. J. A. Shiddiky, D. Dao, Y. Yamauchi, J. A. Rogers, N.-T. Nguyen, *ACS Nano* **2019**, *13*, 11572.
- [12] J. K. Chang, H. P. Chang, Q. Gue, J. Koo, C. I. Wu, J. A. Rogers, *Adv. Mater.* **2018**, *30*, 1704955.
- [13] G. Huang, Y. Mei, *Small* **2018**, *14*, 1703665.
- [14] E. Song, C.-H. Chiang, R. Li, X. Jin, J. Zhao, M. Hill, Y. Xia, L. Li, Y. Huang, S. M. Won, K. J. Yu, X. Sheng, H. Fang, M. A. Alam, Y. Huang, J. Viventi, J. K. Chang, J. A. Roger, *Proc. Natl. Acad. Sci. USA* **2019**, *116*, 15398.
- [15] J. K. Chang, H. Fang, C. A. Bower, E. Song, X. Yu, J. A. Rogers, *Proc. Natl. Acad. Sci. USA* **2017**, *114*, E5522.
- [16] H. Fang, K. J. Yu, C. Gloschat, Z. Yang, E. Song, C.-H. Chiang, J. Zhao, S. M. Won, S. Xu, M. Trumpis, Y. Zhong, S. W. Han, Y. Xue, D. Xu, S. W. Choi, G. Cauwenberghs, M. Kay, Y. Huang, J. Viventi, I. R. Efimov, J. A. Rogers, *Nat. Biomed. Eng.* **2017**, *1*, 0038.
- [17] X. Xu, H. Subbaraman, A. Hosseini, C. Y. Lin, D. Kwong, R. T. Chen, *Opt. Lett.* **2012**, *37*, 1020.
- [18] C. A. Bower, M. A. Meitl, B. Raymond, E. Radauscher, R. Cok, S. Bonafede, D. Gomez, T. Moore, C. Prevatte, B. Fisher, R. Rotzoll, G. A. Melnik, A. Fecioru, A. J. Trindade, *Photonics Res.* **2017**, *5*, A23.
- [19] L. G. P. Martins, Y. Song, T. Zeng, M. S. Dresselhaus, J. Kong, P. T. Araujo, *Proc. Natl. Acad. Sci. USA* **2013**, *110*, 17762.
- [20] J. Seo, C. Kim, B. S. Ma, T. L. Lee, J. H. Bong, J. G. Oh, B. J. Cho, T. S. Kim, *Adv. Funct. Mater.* **2018**, *28*, 1707102.
- [21] M. Kim, A. Shah, C. Li, P. Mustonen, J. Susoma, F. Manoocheir, J. Riikonen, J. Lipsanen, *2D Mater.* **2017**, *4*, 035004.
- [22] C. H. Lee, D. R. Kim, X. Zheng, *ACS Nano* **2014**, *8*, 8746.
- [23] H. Zhou, W. Qin, Q. Yu, H. Cheng, X. Yu, H. Wu, *Nanomaterials* **2019**, *9*, 283.
- [24] C. Linghu, S. Zhang, C. Wang, J. Song, *npj Flexible Electron.* **2018**, *26*, 8247.
- [25] B. Corbett, R. Loi, W. Zhou, D. Liu, Z. Ma, *Prog. Quantum Electron.* **2017**, *52*, 1.
- [26] G. Müller, G. Krötz, E. Niemann, *Sens. Actuators, A* **1994**, *43*, 259.
- [27] T. Nguyen, T. Dinh, A. R. M. Faisal, H.-P. Phan, T.-K. Nguyen, N.-T. Nguyen, D. V. Dao, *Nat. Commun.* **2019**, *10*, 1.
- [28] H.-P. Phan, D. V. Dao, P. Tanner, L. Wang, N.-T. Nguyen, *Appl. Phys. Lett.* **2014**, *104*, 111905.
- [29] T. H. Lee, S. Bhunia, *Science* **2010**, *329*, 1316.
- [30] M. A. Lantz, B. Gotsmann, P. Jaroenapibal, T. D. Jacobs, S. D. O'Connor, K. Sridharan, R. W. Carpick, *Adv. Funct. Mater.* **2012**, *22*, 1639.
- [31] T.-K. Nguyen, H.-P. Phan, T. Dinh, J. Han, S. Dimitrijević, P. Tanner, A. R. M. Faisal, Y. Zhu, N. T. Nguyen, D. V. Dao, *IEEE Electron Device Lett.* **2017**, *38*, 955.
- [32] A. Qamar, H.-P. Phan, T. Dinh, N.-T. Nguyen, M. Rais-Zadeh, *Appl. Phys. Lett.* **2020**, *116*, 132902.
- [33] A. Oliveros, A. Guiseppi-Elie, S. E. Sadow, *Biomed. Microdevices* **2013**, *15*, 353.
- [34] H. Zhuang, N. Yang, L. Zhang, R. Fuchs, X. Jiang, *ACS Appl. Mater. Interfaces* **2015**, *7*, 10886.
- [35] N. Yang, H. Zhuang, R. Hoffmann, W. Smirnov, J. Hees, X. Jiang, C. E. Nebel, *Anal. Chem.* **2011**, *83*, 5827.
- [36] C. A. Diaz-Botia, L. E. Luna, R. M. Neely, M. Charmanzar, C. Carraro, J. M. Carmena, P. N. Sabes, R. Maboudian, M. A. M. Maharbiz, *J. Neural Eng.* **2017**, *14*, 056006.
- [37] F. Deku, Y. Cohen, A. Joshi-Imre, A. Kanneganti, T. J. Gardner, S. F. Cogan, *J. Neural Eng.* **2018**, *15*, 016007.
- [38] S. S. Pandurangi, S. S. Kulkarni, *Int. J. Solids Struct.* **2015**, *62*, 124.
- [39] H.-P. Phan, T.-K. Nguyen, T. Dinh, G. Ina, A. R. Kermany, A. Qamar, J. Han, T. Namazu, R. Maeda, D. V. Dao, N.-T. Nguyen, *Appl. Phys. Lett.* **2017**, *110*, 141906.
- [40] A. R. Kermany, F. Iacopi, *J. Appl. Phys.* **2015**, *118*, 155304.

- [41] P. Tanner, A. Lacopi, H.-P. Phan, S. Dimitrijević, L. Hold, K. Chaik, G. Walker, D. V. Dao, N.-T. Nguyen, *Sci. Rep.* **2017**, *7*, 17734.
- [42] H.-P. Phan, P. Tanner, D. V. Dao, L. Wang, N.-T. Nguyen, Y. Zhu, S. Dimitrijević, *IEEE Electron Device Lett.* **2014**, *35*, 399.
- [43] A. E. Kacimi, E. Pauliac-Vaujour, J. Eymery, *ACS Appl. Mater. Interfaces* **2018**, *10*, 4794.
- [44] N. R. Glavin, K. D. Chabak, E. R. Heller, E. A. Moore, T. A. Prusnick, B. Maruyama, D. E. Walker Jr., D. L. Dorsey, Q. Paduano, M. Snure, *Adv. Mater.* **2017**, *29*, 1701838.
- [45] Y. Liu, H. Wang, W. Zhao, M. Zhang, H. Qin, Y. Xie, *Sensors* **2018**, *18*, 645.
- [46] J. Chun, Y. Hwang, Y. S. Choi, T. Jeong, J. H. Baek, H. C. Ko, S. J. Park, *IEEE Photonics Technol. Lett.* **2012**, *24*, 2115.
- [47] W. F. Quiros-Solano, N. Gaio, C. Silvestri, G. Pandraud, R. Dekker, P. M. Sarro, *Micromachines* **2019**, *10*, 536.
- [48] D. Huh, Y. Torisawa, G. A. Hamilton, H. J. Kim, D. E. Ingber, *Lab Chip* **2012**, *12*, 2156.
- [49] S. Rohmfeld, M. Hundhausen, L. Ley, *J. Appl. Phys.* **2002**, *91*, 1113.
- [50] Y. Mei, P. J. Diemer, J. R. Niazi, R. K. Hallani, K. Jarolimek, C. S. Day, C. Risko, J. E. Anthony, A. Amassian, O. D. Jurchescu, *Proc. Natl. Acad. Sci. USA* **2017**, *114*, E6739.
- [51] J. Lian, Y. Yang, W. Wang, S. G. Parker, V. R. Gonçalves, R. D. Tilley, J. J. Gooding, *Chem. Commun.* **2019**, *55*, 123.